

# Ionic relaxation contribution to the electronic reconstruction at the $n$ -type LaAlO<sub>3</sub>/SrTiO<sub>3</sub> interface

R. Pentcheva<sup>a</sup> and W. E. Pickett<sup>b</sup>

<sup>a</sup>*Department of Earth and Environmental Sciences,  
University of Munich, Theresienstr. 41, 80333 Munich, Germany and*

<sup>b</sup>*Department of Physics, University of California, Davis, CA 95616*

(Dated: June 30, 2008)

Density functional theory calculations reveal that the compensation mechanism at the isolated  $n$ -type interface in LaAlO<sub>3</sub>/SrTiO<sub>3</sub> superlattices involves both ionic and electronic degrees of freedom. Strong ferroelectric distortions screen the local electric field and reduce the band discontinuity across the interface. We find that the electronic reconstruction depends sensitively on whether structural optimization is performed within GGA (conventional exchange and correlation effects) or GGA+U (which includes strong intra-atomic interactions). For a structural optimization within GGA+U the excess charge is confined to the interface TiO<sub>2</sub>-layer with a charge-ordered, orbitally-polarized arrangement of Ti<sup>3+</sup> and Ti<sup>4+</sup>. While the charge ordered phase represents the ground state, optimization within GGA leads to more pronounced ferroelectric distortions, suppression of charge order (with remaining  $d_{xy}$ -orbital occupation in the interface layer) and a delocalization of the excess charge extending over a few SrTiO<sub>3</sub> layers.

PACS numbers: 73.20.-r,73.20.Hb,75.70.Cn,71.28.+d

## I. INTRODUCTION

Correlated electrons in oxide heterostructures open up new possibilities for electronic behavior that is unanticipated from the properties of the bulk constituents and can thus lead to new functionality. Although SrTiO<sub>3</sub> (STO) and LaAlO<sub>3</sub> (LAO) are two conventional nonmagnetic band insulators, their interfaces were reported to be conducting [1]. Recently, there are indications for magnetism [2, 3] and superconductivity [4] in this system at low temperature. These new functionalities lend extra urgency to the effort to understand the unanticipated properties of this interface.

In the perovskite structure there is a natural charge modulation in the [001]-direction, *e.g.* in LaAlO<sub>3</sub> positively charged LaO-layers alternate with negatively charged AlO<sub>2</sub>-layers, while in SrTiO<sub>3</sub> both the SrO and TiO<sub>2</sub>-layers are charge neutral. At both interfaces, the electron-doped  $n$ -type (LaO/TiO<sub>2</sub>) and the hole-doped  $p$ -type (AlO<sub>2</sub>/SrO), local charge neutrality as inferred from the formal valences is disrupted. This seeming violation of charge neutrality has become a central consideration in trying to understand the unexpected behavior that emerges at the interface.

Theoretical studies so far concentrate on explaining the reported conductivity in this system (*e.g.* [5–7]) by considering the ideal (defect-free) interface. However, on the experimental side there is meanwhile a consensus that the oxygen pressure during growth and post annealing plays a crucial role. The initially measured high conductivity is attributed to oxygen defects rather than being an intrinsic

property.[8–11]. Rijnders and Blank [12] related recently the three novel functional properties to three regions of oxygen pressure: (i) high conductivity is measured in samples grown at or below  $p_{O_2} \sim 10^{-6}$  mbar oxygen pressure in the chamber; (ii) superconductivity was found for intermediate pressures of  $p_{O_2} \sim 10^{-4} - 10^{-5}$  mbar; (iii) magnetism and non-conducting behavior was observed only for  $p_{O_2} \sim 10^{-3}$  mbar. The higher oxygen pressure is widely thought to mitigate the formation of oxygen vacancies, resulting in more nearly stoichiometric materials.

In this paper we concentrate on the intrinsic effects in the case where the influence of oxygen defects is minimized and study the (effectively) isolated  $n$ -type interface. Using density functional theory calculations and including a Hubbard  $U$  we have found previously that the charge mismatch at the  $n$ -type LAO/STO interface is accommodated by charge disproportionation on the Ti sublattice in the interface layer with Ti<sup>3+</sup> and Ti<sup>4+</sup> ordered in a checkerboard arrangement [13]. This diluted layer of Ti<sup>3+</sup> spins shows a slight preference for antiferromagnetic coupling [14], as found also for LaTiO<sub>3</sub>/SrTiO<sub>3</sub>-superlattices [15]. First experimental indications for localized magnetic moments at the interface were obtained by Brinkman *et al.* [2] Because the above mentioned calculations were done for a superlattice containing a single unit cell of each material and ideal (bulk) positions of the ions in the cell, we study here the compensation mechanism in more separated interfaces containing thicker slabs of both materials. We focus specifically on the crucial role of lattice relaxations on the electronic

state at the interface, since the largest contribution to the static dielectric constant in both materials arises from the lattice response. In addition we explore how the level of treatment of correlation for the Ti 3d-bands influences the structural and electronic properties at the interface. Furthermore, we calculate the band alignments across the interface using the change of the oxygen O 1s states from the respective bulk materials and the heterostructure.

## II. CALCULATIONAL DETAILS

The DFT-calculations are performed using the all-electron full-potential augmented plane waves (FP-APW) method in the WIEN2k-implementation [16] and the generalized gradient approximation (GGA) [17] of the exchange-correlation potential. Electronic correlations are considered within the fully localized limit (LDA+U) [18] using  $U = 8$  eV and  $J = 1$  eV on the Ti-ions. The muffin tin (MT) radii are:  $R_{\text{La,Sr}}^{\text{MT}} = 2.30$  bohr,  $R_{\text{Ti,Al}}^{\text{MT}} = 1.80$  bohr,  $R_{\text{O}}^{\text{MT}} = 1.60$  bohr. We use a mixed APW+lo and LAPW basis set with the following convergence parameters: Inside the muffin tins wave functions are expanded in spherical harmonics up to  $l_{\text{max}}^{\text{wf}} = 10$  and non-spherical contributions to the electron density and potential up to  $l_{\text{max}}^{\text{pot}} = 4$  are used. The energy cutoff for the plane wave representation in the interstitial is  $E_{\text{max}}^{\text{wf}} = 19$  Ry for the wave functions and  $E_{\text{max}}^{\text{pot}} = 196$  Ry for the potential.

To allow the possibility for more complex symmetry breaking and charge ordering, the calculations are performed in cells with a  $c(2 \times 2)$  lateral periodicity and 15  $k$ -points in the irreducible part of the Brillouin zone. We have used the lateral lattice constant of the SrTiO<sub>3</sub>-substrate obtained from GGA (3.92Å) and  $c = 10a$ . We note that other studies [5–7] have used LDA together with the LDA-lattice parameter (3.84Å), but we choose here the GGA-value also because it is in closer agreement with the experimental lattice constant (3.905Å). Thus the LaAlO<sub>3</sub>-film (3.79Å) is subject to tensile strain on SrTiO<sub>3</sub> due to a lattice mismatch of 3%. To model the superlattice (SL) a symmetric supercell containing only the  $n$ -type interface was chosen in order to avoid internal electric fields resulting from an asymmetric setup. To explore the effect of treatment of electronic correlations on the structural properties a full structural optimization of the internal parameters within the tetragonal unit cell was performed both within GGA and GGA+U [19].

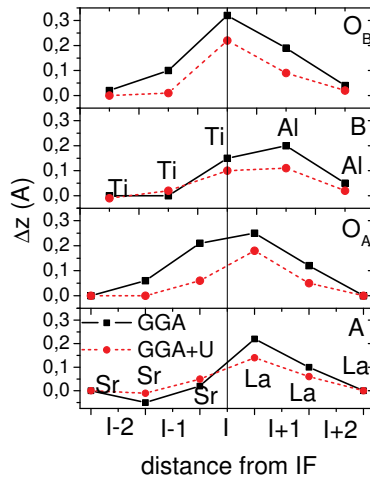


FIG. 1: Vertical displacements of ions  $\Delta z$  in Å in the LAO<sub>4.5</sub>/STO<sub>5.5</sub> superlattice with respect to the bulk positions obtained within GGA (solid black line) and GGA+U (red dashed line). The  $x$  axis shows the distance from the interface (I) TiO<sub>2</sub>-layer. A, B, O<sub>A</sub>, O<sub>B</sub> denote the positions of ions in the layered ABO<sub>3</sub> perovskite lattice.

## III. IONIC RELAXATIONS

While previous studies concentrated on superlattices containing one [13], two [6, 14] and four [5] unit cells of each material, here we investigate the compensation mechanisms in more separated interfaces using a slab containing 4.5 and 5.5 unit cells of the respective bulk compounds as shown in Fig. 2. This system will be denoted LAO<sub>4.5</sub>/STO<sub>5.5</sub> in the following. Generally, displacements from the ideal structure due to strain should affect cations and anions equally, thus giving no ferroelectric (FE) component. Effects that result in differing displacements for cations and anions have a FE character, *i.e.* they produce an electric field or are a response to an electric field, caused in the present case by the change mismatch across the interface.

The lattice relaxations obtained within GGA and GGA+U are presented in Fig. 1. The biggest displacements are observed at the interface where the differences in electronic distribution are largest. Generally, within GGA+U the relaxations are smaller than within GGA and confined closer to the IF with the displacements being more pronounced on the LAO side compared to the STO side. Within GGA, oxygen relaxations are more symmetric across the interface. While both Ti and O in the interface TiO<sub>2</sub> layer move towards the LaO layer, the shifts are stronger for oxygen (0.32Å for GGA; 0.22Å for GGA+U), leading to a distinct ferroelec-

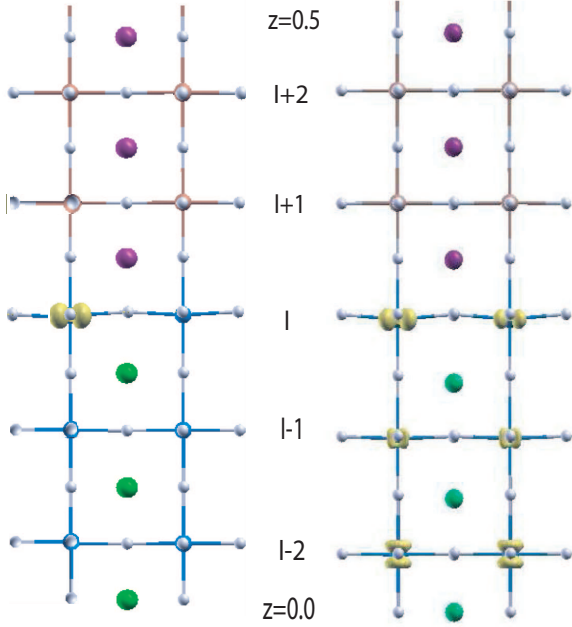


FIG. 2: Crystal structure of a  $\text{LAO}_{4.5}/\text{STO}_{5.5}$  superlattice showing half of the simulation cell with atomic relaxations obtained within (a) GGA+U and (b) GGA. Additionally, the charge density distribution of the occupied Ti 3d-states obtained for both geometries is displayed. For the geometry obtained within GGA+U the Ti 3d-occupation is confined to the interface layer with  $\text{Ti}^{3+}$  and  $\text{Ti}^{4+}$  arranged in a  $c(2 \times 2)$  manner with an occupied  $d_{xy}$  orbital at the  $\text{Ti}^{3+}$ -sites. For b) the strong ferroelectric distortions suppress charge order and delocalize the excess charge throughout the STO-slab, while orbital order ( $d_{xy}$ -partial occupation) is retained in the interface layer.

tric layer distortion of  $0.17\text{\AA}$  (GGA) and  $0.12\text{\AA}$  (GGA+U). These values are similar to FE distortions found in the interface  $\text{TiO}_2$ -layer in LTO/STO superlattices [22, 24] although the direction of Ti-displacement is opposite, which we attribute to the different sign of lattice mismatch. Taking into account the ionic charges, the ferroelectric distortions correspond to a layer-resolved dipole per cell of  $-0.68e\text{\AA}$  (GGA) and  $-0.48e\text{\AA}$  (GGA+U) and a change in potential across the interface  $\text{TiO}_2$  layer of  $0.70$  eV (GGA) and  $0.45$  eV (GGA+U).

Within GGA ferroelectric distortions are observed also in the SrO layer next to the interface, where the Sr-ion remains nearly at its bulk position while the oxygen moves towards the interface by  $0.21\text{\AA}$  leading to a ferroelectric shift between Sr and O of  $0.19\text{\AA}$ . Because both La and O on the other side of the interface shift by  $0.22$  and  $0.25\text{\AA}$ , respectively, the La-Sr separation is elongated by  $0.20\text{\AA}$ .

This value agrees well with the 4.9% elongation inferred from a high-resolution transmission electron microscopy study [20]. While Maurice *et al.* [20] attributed this result to an elongation of the  $\text{TiO}_6$ -octahedron at the interface due to a Jahn-Teller effect, we find no indication for this as both apical oxygens shift by nearly the same amount ( $0.21$  and  $0.25\text{\AA}$ ). On the other hand within GGA+U the ferroelectric distortion is confined to the interface and an elongation of the  $\text{TiO}_6$ -octahedron of  $0.12\text{\AA}$  is observed.

Strong relaxations at the interface were also obtained from pseudopotential calculations using a  $\text{LAO}_{8.5}/\text{STO}_{8.5}$  superlattice [21]. DFT-GGA-studies with smaller simulation cells give qualitatively the same behavior but the actual values of interfacial buckling are smaller ( $0.02$ - $0.10\text{\AA}$ ) [5, 7] and the elongation of the  $\text{TiO}_6$ -octahedron is 2.9% ( $0.11\text{\AA}$ ) [6]. By reducing further the symmetry in a  $\text{LAO}_{1.5}/\text{STO}_{2.5}$  supercell, Zhong and Kelly[14] find indications also for an octahedron tilting.

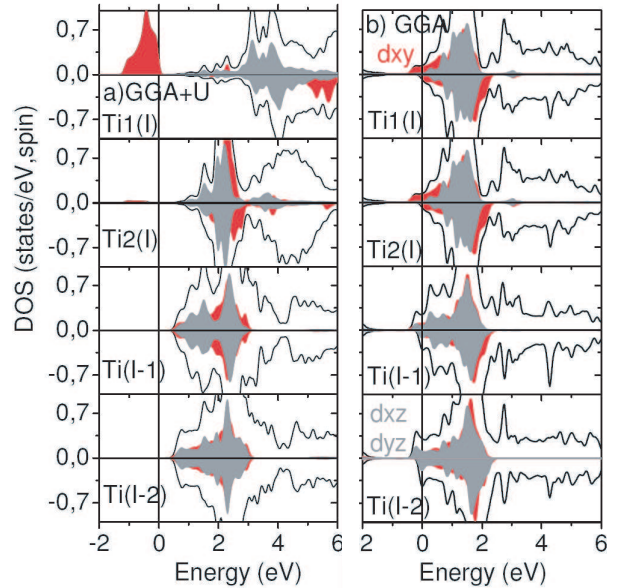


FIG. 3: Layer-resolved density of states of a  $\text{LAO}_{4.5}/\text{STO}_{5.5}$  SL obtained within GGA+U with atomic positions relaxed within a) GGA+U and b) GGA. The two topmost panels show the two Ti-ions at the interface, the succeeding panels show the behavior of the Ti-ions in deeper layers of the STO part of the slab. For the geometry obtained within GGA the excess charge is confined to the IF with a  $\text{Ti}^{3+}$ ,  $\text{Ti}^{4+}$  layer and rapid relaxation of the deeper layers towards bulk behavior away from the interface. The structure relaxed within GGA leads to a metallic STO-part, suppressed charge order and a residual orbital order ( $d_{xy}$ ) at the Ti(I) sites and degenerate  $t_{2g}$  states in deeper layers.

#### IV. ELECTRONIC RECONSTRUCTION

The differences in relaxations obtained within GGA and GGA+U are closely related to the different compensation mechanism of the polar discontinuity at the interface. Here we discuss how relaxations influence the electronic properties. The checkerboard arrangement of  $\text{Ti}^{3+}$  and  $\text{Ti}^{4+}$  at the interface is found both in the  $\text{LAO}_1/\text{STO}_1$ -heterostructure studied previously [13] and the  $\text{LAO}_{4.5}/\text{STO}_{5.5}$  superlattice for the ideal positions of the ions. The structural optimization performed within GGA+U strengthens further the CO state. The spatial distribution of the occupied  $d$ -states in the interface  $\text{TiO}_2$  layer in Fig. 2 shows a disproportionation in  $\text{Ti}^{3+}$  and  $\text{Ti}^{4+}$  with an occupied  $d_{xy}$  orbital (and a magnetic moment of  $0.76\mu_B$ ) at the  $\text{Ti}^{3+}$ -sites. Moreover, the lateral relaxation of oxygen by  $0.04\text{\AA}$  away from  $\text{Ti}^{3+}$  (breathing mode) leads to a further localization of the excess electron and an increase of the gap between the lower Hubbard band ( $d_{xy}$ -orbital) and the unoccupied Ti  $3d$  orbitals from nearly zero to  $0.3\text{ eV}$  as shown in the projected DOS in Fig. 3a.

For comparison we have performed a GGA+U calculation using the geometry obtained in the GGA-optimization. This configuration lies  $0.45\text{ eV}$  above the CO ground state. We find that here the strong relaxations and ferroelectric distortions lead to a suppression of the charge ordering at the interface. As shown both in Fig. 2 and Fig. 3b) the excess charge at the interface becomes more delocalized, resulting in partial occupation of the Ti  $3d$  bands in deeper layers on the STO side. This is in agreement with the suggestion of Hamann *et al.* [22], that the ferroelectric distortion at the IF acts to overscreen the charge in the LaO layer and reduce the trapping of the 2D electron gas at the interface. While at the interface the occupied Ti  $3d$ -states still have  $d_{xy}$ -character, in deeper layers the  $t_{2g}$  orbitals are degenerate. Still, the magnetic moments are almost identical ( $0.14\mu_B$ ) throughout the STO-part.

Thus we find two distinct solutions resulting from a geometry optimization within GGA and GGA+U: a ground state within GGA+U where the excess charge is localized at the interface in a charge ordered and orbitally polarized ( $d_{xy}$ ) insulating state and an energetically higher solution showing stronger ferroelectric distortions from the relaxation within GGA. In the latter case the charge order at the interface is suppressed and the excess charge is delocalized to several STO layers, and the system is metallic. This solution is consistent with other studies (GGA and GGA+U) using a  $(1 \times 1)$ -unit cell [23, 24]. Samples grown at high oxygen pressures ( $\sim 10^{-3}\text{ mbar}$ ) show a sheet resistance at 5 K

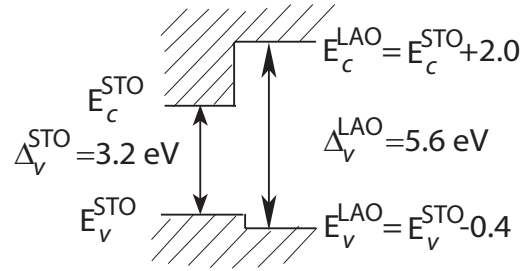


FIG. 4: Schematic picture of the band alignment at the  $n$ -type interface in the  $\text{LAO}_{4.5}/\text{STO}_{5.5}$  superlattice calculated using the O  $1s$  core levels across the interface and the experimental band gaps  $\Delta_{\text{STO}} = 3.2\text{ eV}$  and  $\Delta_{\text{LAO}} = 5.6\text{ eV}$

of  $5 \times 10^4 \Omega/\square$  that is seven orders of magnitude higher than the one for  $p_{\text{O}_2} = 10^{-6}\text{ mbar}$ [2] which suggests a (nearly) insulating ground state. Moreover,  $R_S$  exhibits a logarithmic decrease up to 50 K, which may be consistent with the localization of carriers at  $T=0\text{ K}$  as the CO/OO GGA+U ground state implies.

#### V. BAND DISCONTINUITIES ACROSS THE INTERFACE

The GGA-gap for bulk  $\text{SrTiO}_3$  is  $2.0\text{ eV}$  (experimental value  $3.2\text{ eV}$ ) separating filled O  $2p$  bands and unfilled Ti  $3d$  bands. For  $\text{LaAlO}_3$  we obtain a band gap within GGA of  $3.7\text{ eV}$  (experimental value  $5.6\text{ eV}$ ) between filled O  $2p$  bands hybridized with Al  $p$ -bands and unfilled conduction bands comprised of La  $5d$  and Al  $3s, 3p$  states.

How the bulk band gaps line up across the interface is one of its most fundamental characteristics. Especially when ‘excess’ charge must be accommodated at an interface, the relative positions of the valence band maxima  $E_v$  and conduction band minima  $E_c$  may have a large impact on the charge distribution. In principle these band edges can be identified through the layer projected DOS in successive layers away from the interface. However, valence and conduction wavefunctions, and the local DOS, can be relatively slow to approach their bulk values. For example Albina *et al.* [7] found a difference in the offsets of  $0.1\text{ eV}$  using seven and nine-layer slabs.

A more efficient approach is to use core eigenvalues; in the current system the O  $1s$  eigenvalues are the natural choice. The charge density, and hence the potential, reaches its bulk value more quickly than the Bloch wavefunctions, and hence the core eigenvalues adopt their bulk values only a few layers from the interface.[25] We first determine the valence and conduction band discontinuity from the differ-

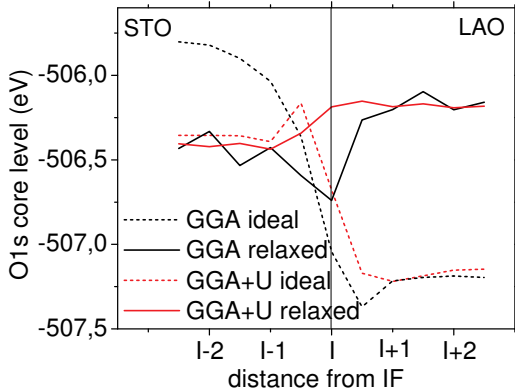


FIG. 5: Positions of O 1s core levels (with respect to the Fermi level) across the interface in the LAO<sub>4.5</sub>/STO<sub>5.5</sub> superlattice before (dashed) and after (solid) relaxation obtained within GGA (black line) and GGA+U (red line). The  $x$  axis shows the distance from the interface (I) TiO<sub>2</sub>-layer. The Fermi levels of all systems are set to zero and only relative variations of the O1s levels from layer to layer are of interest.

ence  $E_v - E_{1s}$  for each bulk compound. To correct for the underestimation of the band gap within GGA, the conduction band discontinuity is obtained by using the experimental band gaps of each compound.

$$\begin{aligned} E_v^{LAO} &= E_v^{STO} - 0.4 \text{ eV}, \\ E_c^{LAO} &= E_c^{STO} + 2.0 \text{ eV}. \end{aligned} \quad (1)$$

The lineup is pictured in Fig. 4. Because the STO-band gap lies completely within the LAO band gap, charge carriers of either sign (electrons or holes) near the interface will go into the STO side of the IF.

The band alignment of the bulk materials is considered to be only one component of the actual band alignment at the interface [26]. To assess the latter, we have plotted in Fig. 5 the  $E_{1s}$  core levels in each layer for the LAO<sub>4.5</sub>/STO<sub>5.5</sub> superlattice. Four cases are displayed: both GGA and GGA+U calculations, each with ideal and with relaxed atomic positions. We note that O 1s energies in the AO and BO<sub>2</sub> layers are distinct near the interface, and attain the (identical) bulk value at only two or three layers from the interface. For the ideal geometry, this effect is slower in GGA than in GGA+U on the STO side. This difference is because in GGA the charge is accommodated over a few STO-layers, while in GGA+U the charge is localized at the interface.

The overriding result is that relaxation, using either method, leads to a large decrease in the varia-

tions in positions of the O 1s core levels across the interface, and the band gap alignment is identical for GGA and GGA+U: the core levels are 0.25 eV higher in LAO than in STO. Although the band line-ups calculated for the relaxed system with GGA and GGA+U are identical, the behavior at the interface layer is very different as discussed in the previous section. It seems to be accidental that the resulting net dipole is exactly the same. Another interesting conclusion is that the band alignment obtained after relaxation of the heterostructure (0.25 eV) is very close to the one suggested from the values of the respective bulk materials (0.4 eV).

## VI. SUMMARY

In summary, we find that the polar discontinuity at the isolated  $n$ -type LAO/STO interface is accommodated both through an intricate combination of ionic relaxation accompanied with electronic reconstruction. The strong ferroelectric distortions lead to a reduction of the valence band discontinuity at the interface compared to the ideal structure and partially compensate the excess charge. This appears to be consistent with the measured lower carrier density of  $1.8 \times 10^{14} \text{ cm}^{-2}$  corresponding to  $\sim 0.27$  electrons per unit cell instead of the expected  $0.5 \text{ e}^-/\text{u.c.}$  [10]. Charge accommodation requires occupation of the Ti 3d band. Within GGA+U the ground state is a charge ordered checkerboard arrangement of  $d_{xy}$  Ti<sup>3+</sup> moments and Ti<sup>4+</sup> localized ions in the interface layer. Lattice relaxations within GGA lead to longer ranged and more pronounced relaxations, and to a suppression of charge order as the excess charge spreads over a few STO layers near the interface. The residual orbital polarization  $d_{xy}$  in the interface TiO<sub>2</sub> layer and the degenerate Ti  $t_{2g}$  bands in deeper layers may lead to interesting transport properties in this system.

## VII. ACKNOWLEDGMENTS

We acknowledge helpful discussions with J. Mannhart, M. Huijben, and J. Eckstein and support through the Bavaria-California Technology Center (BaCaTeC), from DOE Grant DE-FG03-01ER45876, and a grant for computational time at the supercomputer HLRBII at the Leibniz Rechenzentrum.

[1] A. Ohtomo and H. Y. Hwang, Nature **427**, 423 (2004).

[2] A. Brinkman, *et al.*, Nature Mater. **6**, 493 (2007).

- [3] M. van Zalk, *et al.*, cond-mat/0806.4450
- [4] N. Reyren, *et al.*, Science **317**, 1196 (2007).
- [5] S. Gemming and G. Seifert, Acta Mater. **44**, 4299 (2006).
- [6] M.S. Park, S.H. Rhim, and A.J. Freeman, Phys. Rev. B **74**, 205416 (2006).
- [7] J.-M. Albina, M. Mrovec, B. Meyer, and C. Elsässer, Phys. Rev. B **76**, 165103 (2007).
- [8] W. Siemons, G. Koster, H. Yamamoto, W. A. Harrison, G. Lučovský, T. H. Geballe, D. H. A. Blank, and M. R. Beasley, Phys. Rev. Lett. **98**, 196802 (2007)
- [9] N. Nakagawa, H. Y. Hwang, and D.A. Muller, Nature Materials **5**, 204 (2006).
- [10] M. Huijben, G. Rijnders, D. H. A. Blank, S. Bals, S. van Aert, J. Verbeeck, G. van Tendeloo, A. Brinkman, and H. Hilgenkamp, Nature Materials **5**, 556 (2006).
- [11] A. Kalabukhov, R. Gunnarsson, J. Borjesson, E. Olsson, T. Claeson, and D. Winkler, Phys. Rev. B **75**, 121404(R) (2007).
- [12] G. Rijnders and D. H. A. Blank, Nature Materials **7**, 270 (2008).
- [13] R. Pentcheva and W.E. Pickett, Phys. Rev. B **74**, 035112 (2006).
- [14] Z. Zhong and P. Kelly, cond-mat/0801.3160.
- [15] R. Pentcheva and W.E. Pickett, Phys. Rev. Lett. **99**, 016802 (2007).
- [16] P. Blaha, K. Schwarz, G.K.H. Madsen, D. Kvasnicka and J. Luitz, WIEN2k, An Augmented Plane Wave + Local Orbitals Program for Calculating Crystal Properties, (Karlheinz Schwarz, Techn. Univ. Wien, Austria),2001. ISBN 3-9501031-1-2
- [17] J. P. Perdew, K. Burke, and M. Ernzerhof, Phys. Rev. Lett. **77**, 3865, (1996).
- [18] V.I. Anisimov, I.V. Solovyev, M.A. Korotin, M.T. Czyżyk, and G.A. Sawatzky, Phys. Rev. B **48**, 16929 (1993).
- [19] F. Tran, J. Kunes, P. Novak, P. Blaha, and L.D. Marks, submitted to Computer Physics Communications.
- [20] J.-L. Maurice, C. Carretero, M.-J. Casanove, K. Bouzehouane, S. Guyard, E. Larquet, and J.-P. Contour, Phys. Stat. Sol. A **203**, 2209, (2006).
- [21] J.-L. Maurice, I. Devos, M.-J. Casanove, C. Carretero, G. Gachet, D.-G. Crete, D. Imhoff, A. Barthelemy, M. Bibes, K. Bouzehouane, C. Deranlot, S. Fusil, E. Jacquet, B. Domenges, and D. Ballutaud, Mat. Sci. & Eng. B **144**. 1 (2007).
- [22] D. R. Hamann, D.A. Muller, and H.Y. Hwang, Phys. Rev. B **73**, 195403 (2006).
- [23] K. Janicka, J.P. Velev, and E. Tsymbal, Appl. Phys. Lett. **103**, 07B508 (2008).
- [24] S. Okamoto, A. J. Millis, and N. A. Spaldin, Phys. Rev. Lett. **97**, 056802 (2006).
- [25] S. C. Erwin and W. E. Pickett, Solid State Commun. **81**, 891 (1992).
- [26] M. Peressi, N. Blinggeli, and A. Baldareshi, J. Phys. D: Appl. Phys. **31**, 1273 (1998).

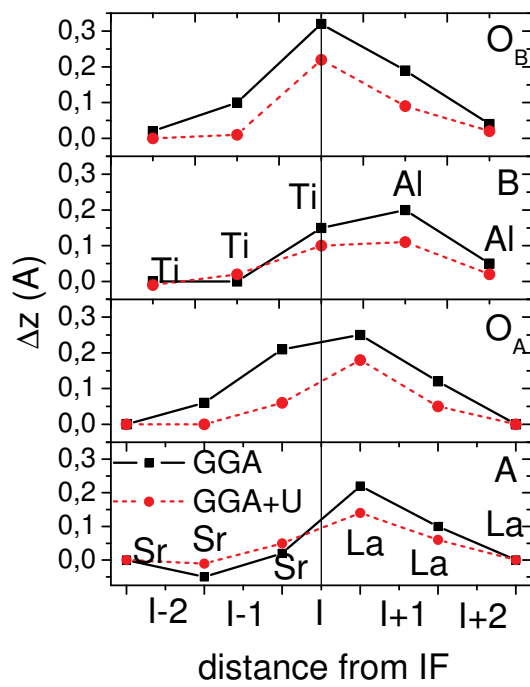


Figure 1

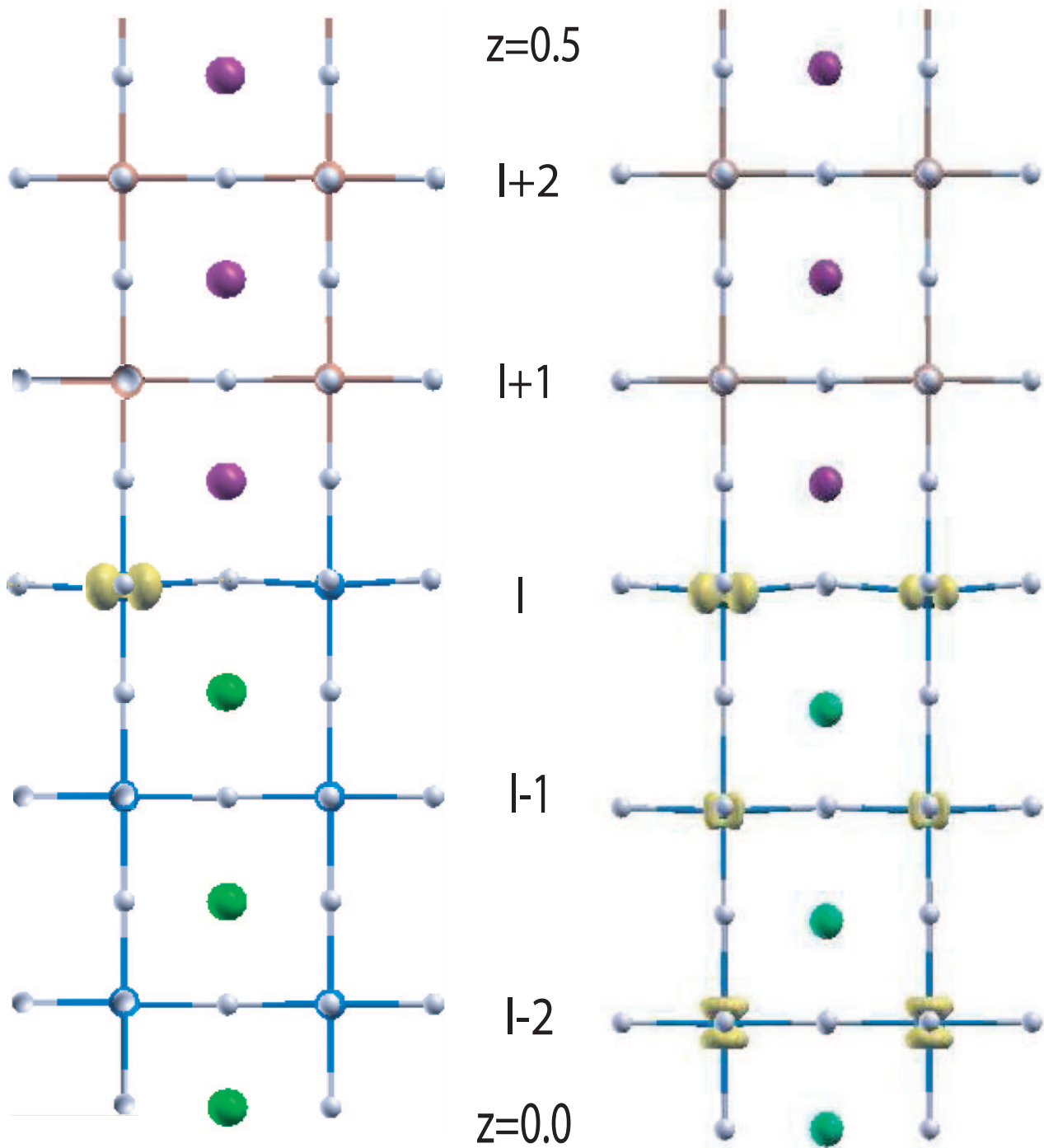


Figure 2

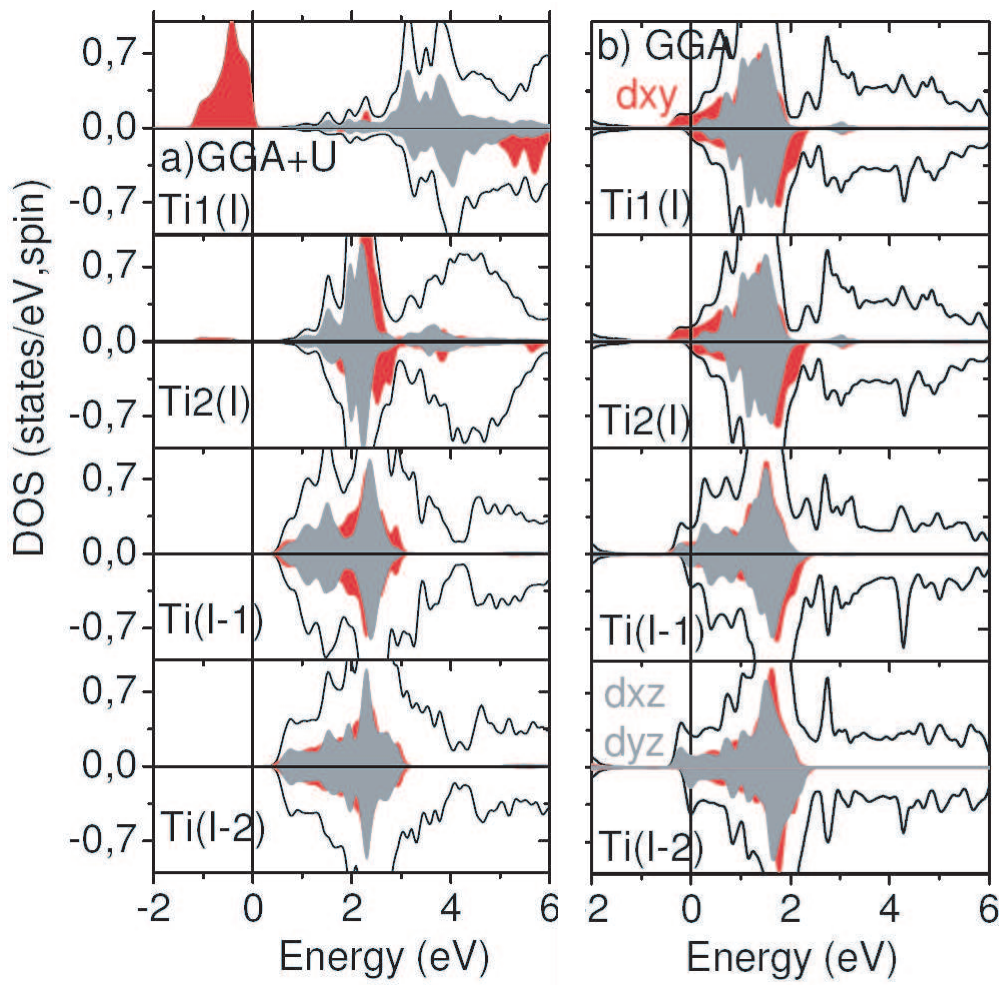


Figure 3

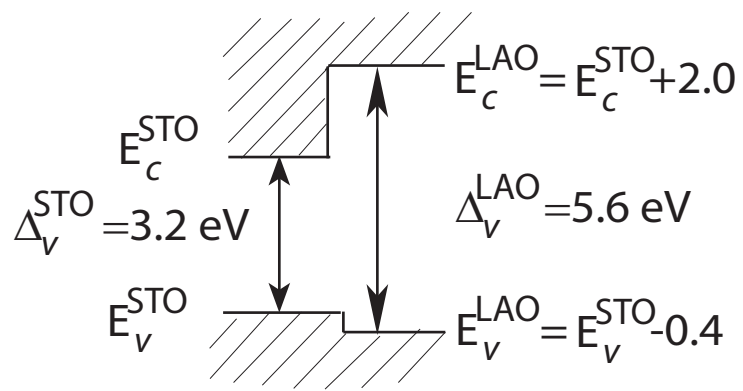


Figure 4

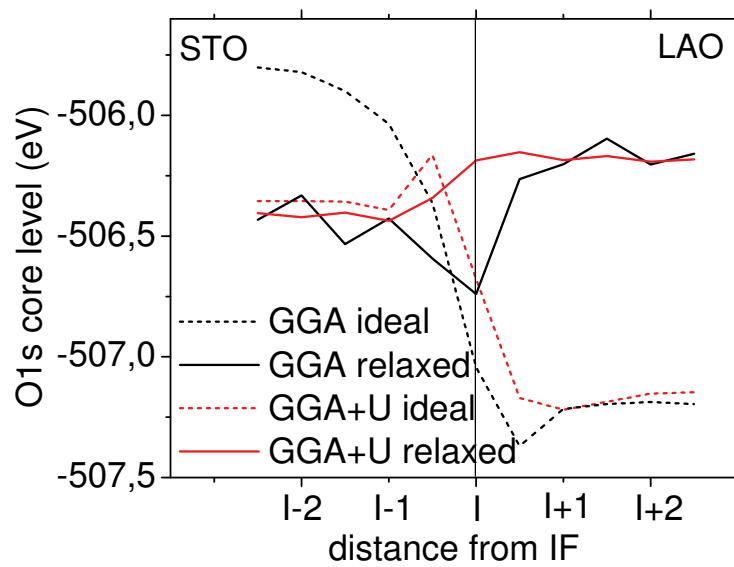


Figure 5